Temperature modeling in a total knee joint replacement using patient-specific kinematics

W.G. Sawyer[a,*], M.A. Hamilton[a], B.J. Fregly[a] and S.A. Banks[b]

[a]Department of Mechanical and Aerospace Engineering, University of Florida, Gainesville, Florida 32611
[b]Orthopaedic Research Lab, The Biomotion Foundation, West Palm Beach, Florida

Received 24 December 2002; accepted 31 March 2003

This paper reports the implementation of a computer modeling approach that uses fluoroscopically measured motions of total knee replacements as inputs and predicts patient-specific implant temperature rises using computationally efficient dynamic contact and thermal analyses. The multibody dynamic simulations of two activities (gait and stair) were generated from the fluoroscopic data to predict contact pressure and slip velocity time histories for individual elements on the tibial insert surface. These time histories were used in a computational thermal analysis to predict average steady-state temperature rise due to frictional heating on each element. For the standard condition, which assumes an ultra-high molecular weight polyethylene (UHMWPE) tibial component and cobalt-chrome femoral component, 1 Hz activity frequency, friction coefficient of $\mu = 0.06$, and convective heat transfer coefficient of $h = 30\,(\mathrm{W}/(\mathrm{m}^2 \cdot \mathrm{K}))$, the predicted maximum temperature rise on the medial compartment was 9.1 and 14 °C for continuous activities of gait and stair respectively. The sensitivity of the temperature rise to activity rate, heat partitioning to the femoral component, and convective heat transfer coefficient was explored. The model is extremely sensitive to the thermal properties of the femoral component and predicts order of magnitude changes in contact temperature with order of magnitude changes in thermal conductivity. A survey of thermal conductivity for current and proposed scratch resistant femoral component implant materials shows variations greater than an order of magnitude.

KEY WORDS: thermal modeling, orthopaedic joint replacements, total knee replacement, friction

1. Introduction

Temperature rise in total hip joint replacements as a result of frictional energy being dissipated at the contact has been measured *in vivo* [1] and *in vitro* [2] and has been modeled using 2-d and 3-d finite element techniques [[3] and [4], respectively]. In the main, the studies conclude that frictional heating may cause temperature rises on the order of 1–10 °C, and that low-friction implant materials are the best way to reduce frictional heating.

In vivo risks associated with frictional heating include increased wear, creep and oxidation degradation of the UHMWPE as well as damage to surrounding biological tissues as a result of the elevated temperatures [5,6]. The over-arching goal of laboratory simulator studies is to exercise component designs in a laboratory environment prior to implantation and to produce results that are relevant and comparable to what will occur when similar components are implanted in patients. These laboratory simulator tests are generally run in diluted bovine serum, which acts as a lubricant and mimics joint synovial fluid. Denaturing of proteins from the serum as a result of frictional heating may coat the components in the simulator and greatly confound the experimental data.

* To whom correspondence should be addressed. E-mail: wgsawyer@ufl.edu

In recent years there has been significant interest in more scratch- and wear-resistant femoral components. The hope is that such components will maintain their initial surface integrity and both the friction and wear of UHMWPE will remain low. These materials are being selected for femoral components of both knee and hip replacements. The purpose of this study is to present a thermal analysis for the UHMWPE tibial component of total knee replacements and discuss the sensitivity of frictional heating to activity frequency, thermal conductivity of the femoral component, and heat transfer coefficient of the synovial fluid.

2. Collection of patient kinematics and modeling of joint contact

Fluoroscopic kinematic data were collected from one total knee arthroplasty patient: female, age 65 at time of surgery, height 170 cm, mass 70 kg [7]. The implanted component was a cemented posterior cruciate ligament-retaining prosthesis (Series 7000, Stryker Howmedica Osteonics, Inc, Allendale, NJ) with a 6.8 mm thick insert. The Knee Society Clinical Rating System scores for this patient [8] were 97-knee and 80-function after one year and 99-knee and 100-function after two years.

The patient performed treadmill gait and stair rise/descent activities during fluoroscopic motion analysis [9–12] 21 months after surgery. Fluoroscopic analysis

1023-8883/03/1100–0343/0

matches three-dimensional models of the prosthetic components to the two-dimensional fluoroscopic images. The technique is accurate to approximately 1° for all rotations and 0.5 mm for translations in the sagittal plane [10]. Kinematic data from one representative cycle of each activity was averaged in 5° increments of knee flexion for stair and 1% increments for gait, including stance and swing phases.

A multibody dynamic contact model was constructed by coupling a commercial software program (Pro/Mechanica Motion, Parametric Technology Corporation, Waltham, MA) with custom elastic contact model software [13]. The contact model utilized elastic foundation theory [14–17] for the tibial component, which is modeled as an elastic layer of known thickness. The femoral component is assumed to be rigid. The contact pressure, P_i, for any tibial element can be calculated using equation (1) [14–16]:

$$P_i = \frac{(1-\nu_t)E_t}{((1+\nu_t)(1-2\nu_t))h_t}\delta. \quad (1)$$

In equation (1), E_t is Young's modulus of the elastic layer, ν_t is Poisson's ratio of the layer, h_t is the thickness of the element, and δ is the interpenetration of the undeformed surfaces in the direction of the local surface normal.

The dynamic contact model used *in vivo* fluoroscopic measurements (anterior–posterior translation, internal–external rotation, and flexion; figure 1(a), (b), and (c), respectively) as prescribed kinematic inputs. The model predicted the remaining three degrees of freedom (axial translation, varus-valgus rotation, and medial-lateral translation) via forward dynamic simulation to ensure compatibility with the applied loads. All prescribed and predicted motions were for the femur moving with respect to a fixed tibia.

The axial force was applied vertically downward onto the femoral component and positioned to produce a 70–30 medial-lateral load split at 0° flexion [18–20]. Leg realignment and ligament balancing are performed during knee replacement surgery to produce a 50–50 load split under static unloaded conditions. However, under dynamic loaded conditions such as gait and stair rise, the center of mass of the body is cantilevered over the support leg, resulting in knee moment that produces greater loads on the medial side. For this study, measured vertical forces during gait and stair activities from a patient of similar age, height, weight, and knee flexion characteristics were used [21]. The axial force curve for gait and stair, figure 1(d), was defined by scaling the vertical ground reaction force curve [17,22,23] to be between 0.25 and 3.0 BW [17,19,22,23].

The dynamic contact model generated contact pressures and slip velocities in two steps. First, a forward dynamics simulation calculated contact forces and kinematics using a 35×20 element grid on each tibial insert contact surface. The precision of the results was verified by repeating the simulation with a denser 50×35 element grid. Then an inverse dynamics analysis used the results from the forward dynamics simulation to calculate contact pressures and slip velocities over a square 50×50 element grid for improved visualization.

3. Thermal modeling

The thermal modeling begins by assuming a particular partitioning of energy Q (J) into the femoral component Q_f and tibial component Q_t respectively. Equation (2) gives an expression for the energy dissipated in the contact, where μ is the friction coefficient, F is the normal load, V is the slip speed, T is the total activity time, and τ is an instant in time during the activity:

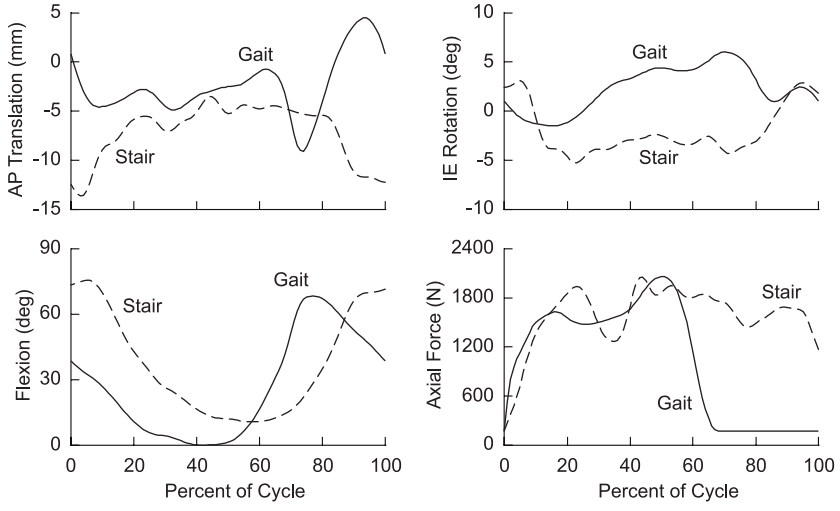

Figure 1. Kinematic and load inputs into the dynamic contact model: AP translation, IE rotation, flexion, and axial force.

$$Q = Q_f + Q_t = \mu \int_0^T F_\tau |V_\tau| \, d\tau. \tag{2}$$

The energy is partitioned into the two bodies as shown in figure 2 and given by equation (3). The energy partition rule is based on matching the interface temperature for: (a) stationary contact area of two half-spaces and (b) femoral component moving relative to a stationary tibial component. Both the femoral component and tibial component are modeled as half-spaces of thermal conductivities k_f and k_t respectively. Partitioning heat based on a moving heat source (b) is generally preferred when the Peclet number, Pe, is greater than 10 [25,26]:

$$Pe < 10 \quad Q_t = Q\left(1 + \frac{k_f}{k_t}\right)^{-1}, \qquad Q_f = Q\left(1 + \frac{k_t}{k_f}\right)^{-1}$$

$$Pe > 10 \quad Q_t = Q\left(1 + \frac{k_f}{k_t}\frac{\sqrt{Pe_f}}{1.6}\right)^{-1},$$

$$Q_f = Q\left(1 + \frac{k_t}{k_f}\frac{1.6}{\sqrt{Pe_f}}\right)^{-1}. \tag{3}$$

The Peclet number for the femoral component is defined as $Pe_f = V_f l/\alpha_f$, where V_f is a characteristic sliding speed of the femoral component, l is a characteristic half-width of the contact patch, and α_f is the thermal diffusivity of the femoral component. From equation (3) it can readily be seen that the moving source partitions greater heat into the femoral component for $Pe_f > 1$. A stationary partitioning of heat is assumed for the remainder of the modeling and analysis, in part because partitioning greater amounts of heat into the tibial component should provide an upper bound on the frictional heating likely to be seen in service.

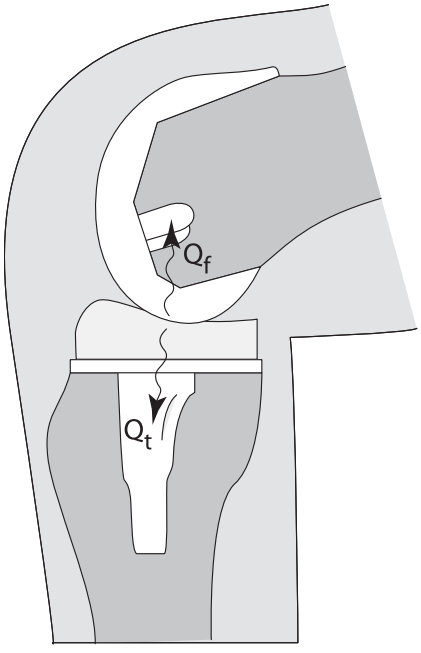

Figure 2. Schematic of the knee joint showing the partitioning of energy into the femoral and tibial components.

The heat flux $\dot{q}_i$ (W/m^2) is found for a tibial element i by partitioning the average energy dissipated over that element and dividing by the activity time. This is shown in equation (4), where P_τ is the pressure on element i at time τ:

$$\dot{q}_i = \frac{\mu}{T\left(1 + \frac{k_f}{k_t}\right)} \int_0^T P_\tau |V_\tau| \, d\tau. \tag{4}$$

The temperature rise θ_λ at a particular element λ is found using the algorithm shown schematically in figure 3 and given by equation (5). This algorithm is for square elements of area A and half-width a, and the vector from the origin element λ to element i is $\vec{r}_{\lambda i}$.

$$\theta_\lambda = 1.12\frac{\dot{q}_\lambda a_\lambda}{k_t} + \sum_{i=0}^{n;i\neq\lambda} \frac{\dot{q}_i A_i}{2\pi k_t |\vec{r}_{\lambda i}|}. \tag{5}$$

The first group in the algorithm is the central temperature rise of the square element under uniform heat flux $\dot{q}_\lambda$. The second group in the algorithm is the summation of all of the contributions of the remaining surface elements to the temperature rise. This algorithm treats all of the contributing elements as a single point source of heat, $\dot{Q}_i = \dot{q}_i A_i$, and uses the classic point source solution discussed in detail in Carslaw and Jaeger [24]. This algorithm is used for all elements regard-less of whether or not they experience a frictional heat flux.

The elements that do not experience a frictional heat flux during the activity are exposed to the synovial fluid, and convective cooling of the component occurs through this surface/fluid interface. The heat flux of these elements not in contact is assumed to follow Newton's law of cooling, as shown in equation 6, where θ_i is the temperature rise of the element above ambient temperature, $\theta_i = T_s - T_{\text{amb}}$, and h is the convection heat transfer coefficient with units of W/(m$^2 \cdot$ K):

$$\dot{q}_i = -h\theta_i. \tag{6}$$

The solution for the surface temperature map of the tibial component requires an iterative solver due to the coupling between the convective cooling heat flux and the surface temperature. The solution approach is similar to a fixed-point iteration with two constraints on the solution method: (1) the convective cooling power cannot exceed the frictional heat and (2) surface temperatures below ambient are not permitted.

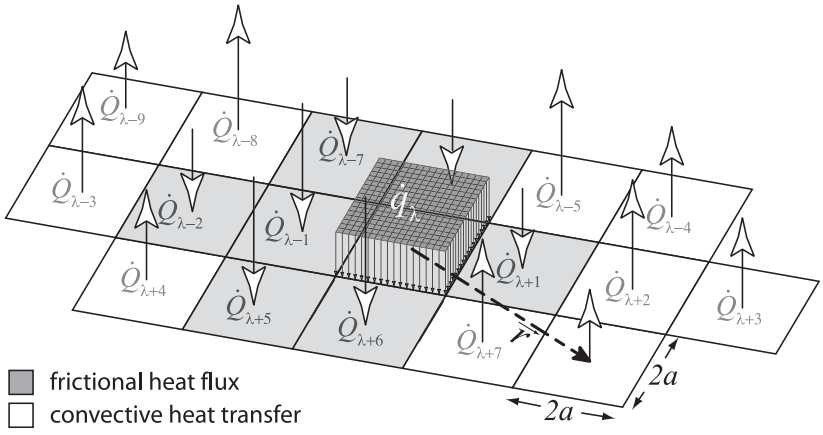

Figure 3. Schematic of the solution approach for temperature rise of element λ, with neighboring elements treated as point sources of heat (both frictional heating and convective cooling).

4. Results and discussion

The values of the various variables needed in this code that defines the '*standard condition*' for both gait and stair rise activities are given in table 1. The standard condition assumes a 1 Hz activity with a cobalt-chrome femoral component, a low convective heat transfer coefficient, and a low Peclet number partitioning of heat.

The heat flux contour plot as described by equation (4) is shown in figure 4(a) and 5(a) for the gait and stair activities respectively. The resulting temperature-rise contour plots are shown in figure 4(b) and 5(b) for the gait and stair activities respectively. These temperature results converge quickly, less than 100 iterations. For both gait and stair rise activity maximum temperature occurs on the medial compartment.

The code was run varying three different parameters off of the standard condition; these were activity frequency, heat transfer coefficient, and thermal conductivity of the femoral component. Table 3 summarizes these data.

The choice of femoral component thermal conductivity for the standard condition corresponds to a cobalt-chrome component, which is widely used. The maximum contact temperature is extremely sensitive to the choice of femoral component thermal conductivity. At $k_f = 0.4$ half of the frictional heating is carried away by the femoral component and half goes into the tibial component. At $k_f = 40.0$ only 1% of the frictional heating goes into the tibial component.

The stationary analysis partitions heat to the respective bodies as a function of their thermal conductivities only. This is considered reasonable for low values of the Peclet number. However, for the standard condition (cobalt-chrome femoral component) characteristic sliding speed is $V_f = 0.100\,\text{m/s}$, representative contact half-length is $l = 0.002\,\text{m}$, and the thermal diffusivity is $\alpha_f = 3.4 \times 10^{-6}$, thus $Pe_f \approx 60$. The energy partition and corresponding maximum temperature rise for this standard condition are $Q_t = 3\%Q_{\text{total}}$ and $\theta_{\max} = 10.5^\circ\,\text{C}$ and $Q_t = 0.6\%Q_{\text{total}}$ and $\theta_{\max} = 2.5\,^\circ\text{C}$ for stationary and moving analysis respectively. In figure 6(b) the upper horizontal axis, x_2, gives the ratio of the heat going into the tibial component to the total frictional heat; thus the graph can be used to calculate temperature rise for any partitioning of energy over the range $Q_t = 1\%Q_{\text{total}}$ to $Q_t = 50\%Q_{\text{total}}$.

The activity frequencies were varied between 0.5 and 2 Hz. The nearly linear trend of frictional heating with activity frequency (figure 6(a)) is expected. This can be most easily seen in equation (4), where the frictional heat flux is directly proportional to the sliding speed.

Table 1
Values and references for the various constants used by the code for the '*standard condition*'.

	Value	Units	Reference(s)
Elastic modulus E	460.00	MPa	[27]
Poisson's ratio ν	0.46		[28]
Thermal conductivity			
tibial component k_t	0.40	W/(m · K)	
femoral component k_f	13.00	W/(m · K)	
Convection coefficient h	30.00	W/(m^2 · K)	[29]
Cycle time (stair & gait) T	1.00	s	
Friction coefficient μ	0.06		[30]

The elastic modulus and Poisson's ratio are for the UHMWPE, as the femoral component is assumed to be rigid for the contact analysis.

Table 2
Thermal conductivities of various materials as provided by suppliers.

	Thermal conductivity k, W/(m · K)
Alumina	25.00
Cobalt-Chrome	13.00
Stainless-Steel 316L	15.00
Ti-6Al-4V	6.70
Zirconia	1.70
Zirconium	65.00
UHMWPE	0.40

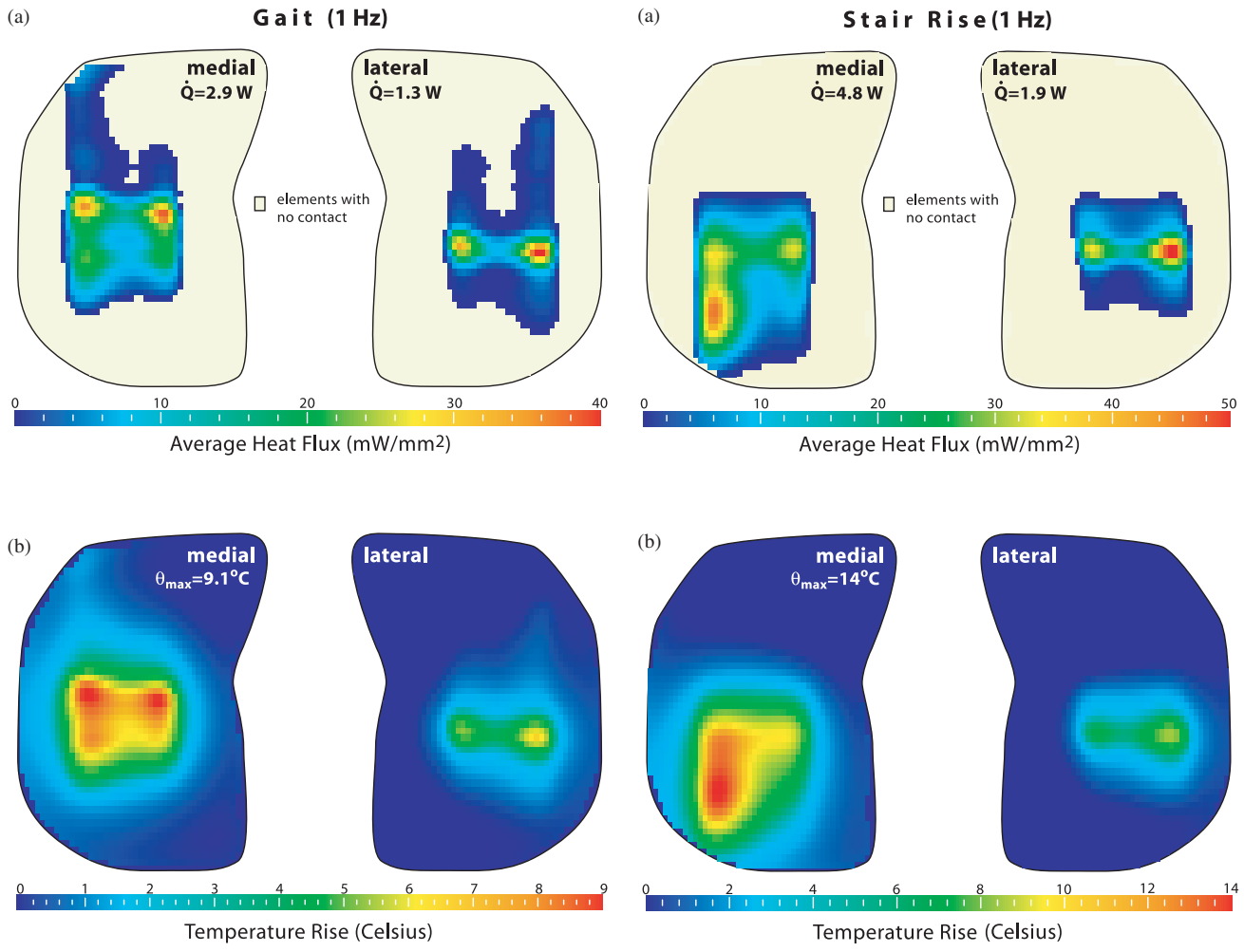

Figure 4. Contour maps for continuous stair activity for the '*standard condition*' of (a) the average frictional heat flux and (b) the temperature rise in °C. (1 Hz, $k_f = 13\,\mathrm{W/(m \cdot K)}$, $\mu = 0.06$, $h = 30(\mathrm{W/(m^2 \cdot K)})$.

Figure 5. Contour maps for continuous stair activity for the '*standard condition*' of (a) the average frictional heat flux and (b) the temperature rise in °C. (1 Hz, $k_f = 13\,\mathrm{W/(m \cdot K)}$, $\mu = 0.06$, $h = 30(\mathrm{W/(m^2 \cdot K)})$.

The activity period is proportional to the kinematic path, which is essentially constant, divided by the speed. Activity frequency is the reciprocal of the activity period; thus, activity frequency is directly proportional to speed. Similarly, though not shown, linear dependencies with friction coefficient were expected and found.

The very weak dependence on the convection coefficient (figure 6(c)) is somewhat surprising, but perhaps fortuitous. Because the frictional heat flux was discretized and time averaged for the various elements, the tibial surface has islands of frictional heating surrounded by regions of convective cooling. Any element that experiences contact is precluded from providing cooling. During these activities, elements are continuously exposed to both frictional heating and convective cooling. This mixture of heating and cooling would yield a lower average heat flux than that used by this solution procedure.

In vivo the knee does not go for thousands of cycles without a break. As discussed above, this steady-state analysis takes average heat fluxes to predict the contact temperature. The time required for this system to reach steady-state was not explored. Thus, many interrupted activities may not reach the temperatures predicted here. The analysis is more similar to joint simulator machines that can run for hours or days without stopping.

The reasonableness of these results is interesting given that many studies on the temperature rises for hip replacements find 1–10 °C and the present results for the knee replacement are generally in line with those findings. While most previous studies have looked at activity frequency and friction coefficient, it is interesting to see the predicted strong dependency on the femoral component thermal conductivity. Figure 7 takes the results shown in figure 6(b) and locates the various materials listed in table 2. And while promoting the reasonableness of the results around the '*standard condition*,' the unreasonable predictions for materials with low thermal conductivities should be noted. This a clear indication of the problems that arise when using half-space models for this type of analysis, and, perhaps, in the future such limitations can be addressed using finite element analysis.

Table 3
Conditions run off of the '*standard condition*' (bold) and corresponding maximum temperature rise in degrees Celsius for the gait and stair activities accordingly.

Cycle frequency (Hz)	Femoral component thermal conductivity k_f (W/m·K))	Convection heat transfer coefficient h (W/(m^2·K))	Maximum temperature rise	
			Gait θ_{max} (°C)	Stair θ_{max} (°C)
Frequency excursions				
1/2	13.0	30.0	4.5	7.2
3/4	13.0	30.0	6.8	11.0
1	**13.0**	**30.0**	**9.1**	**14.0**
1 1/4	13.0	30.0	11.0	18.0
1 1/2	13.0	30.0	14.0	22.0
1 3/4	13.0	30.0	16.0	25.0
2	13.0	30.0	18.0	29.0
Thermal conductivity excursions				
1	0.40	30.0	150.0	240.0
1	1.3	30.0	71.0	110.0
1	4.0	30.0	28.0	44.0
1	**13.0**	**30.0**	**9.1**	**14.0**
1	40.0	30.0	3.0	4.8
Convection heat transfer excursions				
1	13.0	1.0	10.0	16.0
1	13.0	3.0	10.0	16.0
1	13.0	10.0	9.7	15.0
1	**13.0**	**30.0**	**9.1**	**14.0**
1	13.0	100.0	6.5	11.0

Overall the analysis here aims to provide a simple first model for thermal analysis during continuous activities such as gait and stair for total knee replacements with UHMWPE tibial bearings. The findings from the standard conditions are most likely overestimates of actual steady-state temperature rises, primarily because of the heat partitioning and time averaging of the heat-flux, which precludes frictional heating and convective cooling to operate on the same element.

5. Conclusions

(1) Average heat flux patches are calculated for the medial and lateral compartments of the UHMWPE tibial component for gait and stair activities, and a simple argument for partitioning of heat based on the assumption of two stationary half-spaces is offered as a first approach to predicting *in vivo* frictional heating values.
(2) A thermal model for the frictional temperature rise on the surface of the tibial component suggests temperature rises below 10 °C during continuous activities such as gait and stair rise.
(3) The temperature increases with increasing activity rate, decreasing heat transfer coefficient, and decreasing thermal conductivity of the femoral component.
(4) The predicted strong sensitivity of temperature rise to femoral component thermal conductivity suggest that thermal conductivity should be a consideration when selecting next-generation scratch-resistant femoral components.
(5) The analysis here chose conditions for the most common material combinations to provide an upper bound for the frictional heating temperatures experienced *in vivo*.

Appendix: Analytical transient analysis without convection

The analysis presented in this manuscript was developed for steady-state conditions; it is of interest to estimate the time to reach steady-state. In this Appendix an analytical model is presented for a square heat flux of intensity $\dot{q}$(W/m^2) and area $4a^2$. The analysis begins from the time-dependent solution of the incremental temperature rise $d\theta$(K) for a continuous point source of intensity $d\dot{Q}$(W), located some distance r(m) from the point of interest; in this analysis the location of interest will be the origin, which corresponds to a point at the centroid of the square heat source on the surface. This analysis follows the work of Carslaw and Jaeger (1959) [24].

$$d\theta = \frac{d\dot{Q} erfc\left(\frac{r}{\sqrt{4\alpha t}}\right)}{2k\pi r}. \tag{A.1}$$

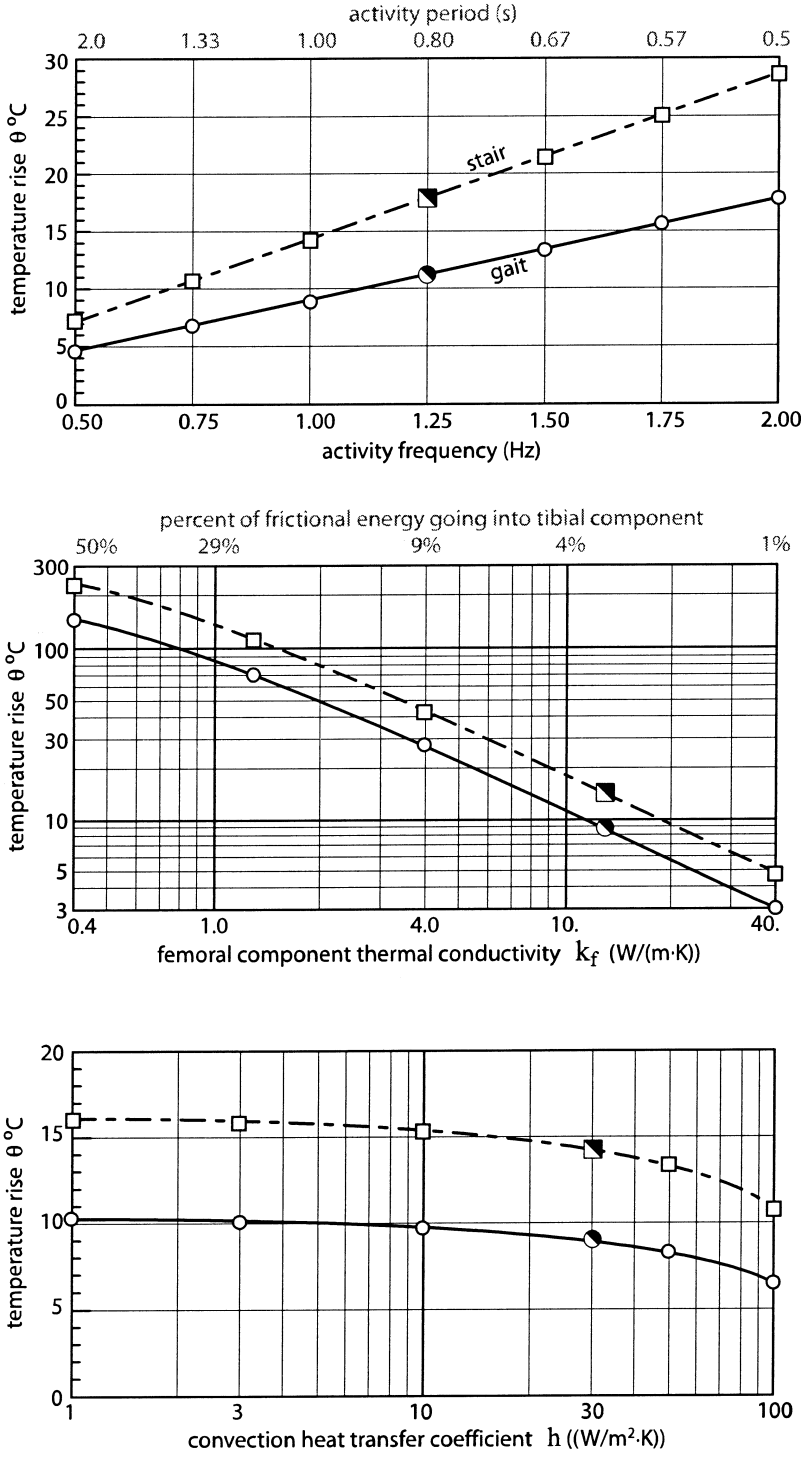

Figure 6. Plots of maximum temperature for variations in (a) activity rate, (b) thermal conductivity of the femoral component, and (c) convection heat transfer coefficient.

In equation (A.1), $\alpha\,(\mathrm{m}^2/\mathrm{s})$ is the thermal diffusivity, $k\,(\mathrm{W}/(\mathrm{m}\cdot\mathrm{K}))$ is the thermal conductivity, and $t\,(\mathrm{s})$ is time that the source has been acting. To find the time-dependent temperature rise at the origin θ_o due to a uniform square heat flux, equation (A.1) is integrated over a range of differential heat sources from $x = -a \to a$ and $y = -a \to a$. This is shown in equation (A.2), where $r = \sqrt{x^2 + y^2}$ and $d\dot{Q} = \dot{q}\,dx\,dy$ ($\dot{q}$ is the heat flux $\left(\mathrm{W}/\mathrm{m}^2\right)$):

$$\theta_o = \frac{\dot{q}}{2k\pi} \int_{-a}^{a} \int_{-a}^{a} \frac{\operatorname{erfc}\left(\dfrac{\sqrt{x^2+y^2}}{\sqrt{4\alpha t}}\right)}{\sqrt{x^2+y^2}}\,dx\,dy. \qquad \text{(A2)}$$

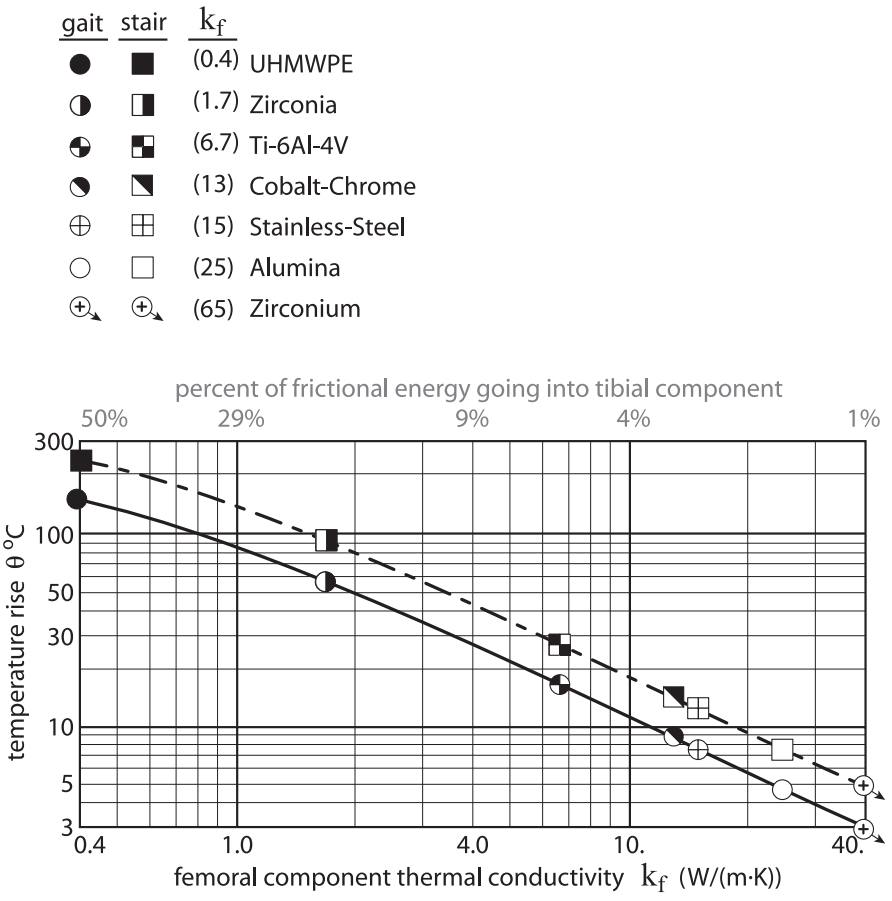

Figure 7. Plot of maximum temperature for variations in thermal conductivity with femoral component materials taken from table 2.

The complementary error function, which appears in equation (A.1) and (A.2), goes to unity as time goes to infinity. Thus these two equations can be easily simplified for the steady-state temperature rise at the origin $\theta_{o_{\text{steady-state}}}$ as shown in equation (A.3):

$$\theta_{o_{\text{steady-state}}} = \frac{\dot{q}}{2k\pi} \int_{-a}^{a} \int_{-a}^{a} \frac{1}{\sqrt{x^2+y^2}}\, dx\, dy. \qquad \text{(A.3)}$$

A dimensionless temperature rise is given by equation (A.4), where the temperature rise at the origin is normalized by the steady-state value; thus the range in dimensionless temperature rise is from 0 to 1:

$$\tilde{\theta}_o = \frac{\theta_o}{\theta_{o_{\text{steady-state}}}}. \qquad \text{(A.4)}$$

The integrals shown in equations (A.2) and (A.3) are evaluated under the *'standard condition'* without convection for the medial compartment during gait. The material properties of the UHMWPE needed for the analysis are $k = 0.4$ and $\alpha = 2 \times 10^{-7}$. A square area of dimension 14 mm × 14 mm is a relatively good fit to the medial compartment's heat flux area during gait (the square half-width is set to $a = 7$ mm for this analysis). The average medial compartment heat flux during gait is calculated to be approximately 15 mW/mm^2. Finally, the *'standard condition'* partitioning directs approximately 3.5% of this total heat flux into the UHMWPE half-space. This analytical solution methodology assumes an insulated surface and therefore corresponds to the condition of $h = 0$. The resulting steady-state temperature rise at the origin with the appropriate numerical substitutions is given by equation (A.5):

$$\theta_{o_{\text{steady-state}}} = \frac{(0.035)15{,}000}{2(0.4)\pi} \int_{-0.007}^{0.007} \int_{-0.007}^{0.007} \times \frac{1}{\sqrt{x^2+y^2}}\, dx\, dy = 10.3\,^{\circ}\text{C}. \qquad \text{(A.5)}$$

The temperature rise of 10.3 °C corresponds well to the calculated temperature rise shown in figure 6(c), which predicts a temperature rise just over 10 °C when the convective heat transfer coefficient is $h = 1$. Figure 8 shows the time-dependent normalized temperature rise from 0.1–100 minutes. It is interesting to note that the central location achieves nearly 66% of its steady-state

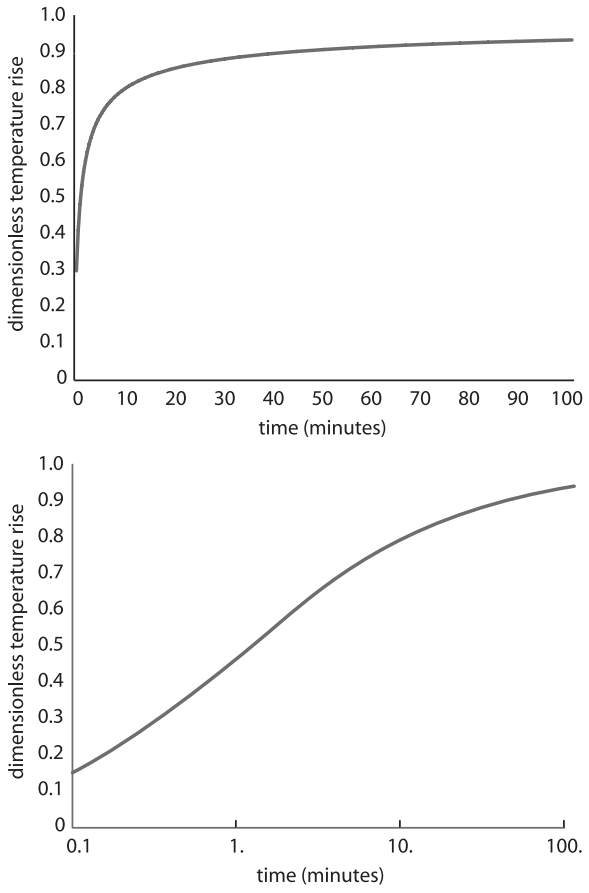

Figure 8. Plots of maximum normalized temperature versus time: (a) linear; (b) logarithmic.

value in the first 3 min. However, this analysis neglects the cooling effects due to convection, which would increase the time to steady-state.

References

[1] G. Bergmann, F. Graichen, A. Rohlmann, N. Verdonschot and G. H. van Lenthe, J. Biomech. 34 (2001a) 421.

[2] Y.S. Liao, Z. Lu, P.D. Benya and H.A. McKellop, in: *Proceedings of the 48th Annual Meeting of the Orthopaedic Research Society*, February, Dallas, Texas (2002).

[3] C.C. Hu, J.J. Liau, C.Y. Lung, C.H. Huang and C.K. Cheng, Mat. Sci. Eng. C 17 (2001) 11

[4] G. Bergmann, F. Graichen, A. Rohlmann, N. Verdonschot, and G.H. van Lenthe, J. Biomech. 34 (2001b) 429.

[5] J.A. Davidson, G. Schwartz and G. Lynch, J. Biomed. Mat. Res. 21 (1987) 261.

[6] J.A. Davidson, G. Schwartz and G. Lynch, J. Biomed. Mat. Res. 22 (1988) 69.

[7] M.K. Harman, S.A. Banks and W.A. Hodge, Clin. Orthopaedics Rel. Res. 392 (2001).

[8] J.N. Insall, L.D. Dorr, R.D. Scott and W.N. Scott, Clin. Orthopaedics Rel. Res. 248 (1989) 13.

[9] S.A. Banks, Ph.D. Dissertation, Massachusetts Institute of Technology, Cambridge, MA. (1992).

[10] S.A. Banks and W.A. Hodge, IEEE Trans. Bio. Eng. 43 (1996) 638.

[11] S.A. Banks, G.D. Markovich and W.A. Hodge, J. Arthroplasty 12 (1997a) 297.

[12] S.A. Banks, G.D. Markovich and W.A. Hodge, Am. J. Knee Surg. 10 (1997b) 261.

[13] B.J. Fregly, Y. Bei, and M.E. Sylvester, J. Biomech. (accepted) (2003a).

[14] K.L. Johnson, *Contact Mechanics* (Cambridge University Press, Cambridge, 1985).

[15] K.N. An, S. Himenso, H. Tsumura, T. Kawai and E.Y.S. Chao, J. Biomech. 23 (1990) 1013.

[16] L. Blankevoort, J.H. Kuiper, R. Huiskes and H.J. Grootenboer, J. Biomech. 24 (1991) 1019.

[17] T.-W. Lu, S.J.G. Taylor, J.J. O'Connor and P.S. Walker, J. Biomechanics 30 (1997) 1101.

[18] F. Johnson, P. Scarrow, and W. Waugh, Med. Biolog. Eng. Comp. 19 (1981) 237.

[19] O.D. Schipplein and T.P. Andriacchi, J. Orthopaedic Res. 9 (1991) 113.

[20] D.E. Hurwitz, D.R. Sumer, T.P. Andriacchi and D.A. Sugar, J. Biomech. 31 (1998) 423.

[21] S.A. Banks, J.C. Otis, S.I. Backus, G.L. Furman and S.B. Haas, in: *Proceedings of the 67th Annual Meeting of the American Academy of Orthopaedic Surgeons*, March, Orlando, Florida (2000).

[22] S.J.G. Taylor, P.S. Walker, J.S. Perry, S.R. Cannon and R. Woledge, J. Arthroplasty 13 (1998) 428.

[23] S.J.G. Taylor and P.S. Walker, J. Biomech. 34 (2001) 839.

[24] H.S. Carslaw and J.C. Jaeger, *Conduction of Heat in Solids* (Oxford University Press, Oxford, 1959).

[25] J.A. Williams, *Engineering Tribology* (Oxford University Press, Oxford, 1998).

[26] B. Bhushan, *Principles and Applications of Tribology* (John Wiley and Sons, New York, 1999).

[27] S.M. Kurtz, C.W. Jewett, J.S. Bergström, J.R. Foulds and A.A. Edidin, Biomaterials 23 (2002) 1907.

[28] D.L. Bartel, J.J. Rawlinson, A.H. Burstein, C.S. Ranawat and W.F. Flynn, Clin. Orthopaedics Rel. Res. 317 (1995) 76.

[29] S. Kakaç and Y. Yener, *Convective Heat Transfer* (CRC Press, Boca Raton, Florida, 1995).

[30] R.M. Hall and A. Unsworth, Biomaterials 1997 (1997) 1017.